Published in final edited form as:
Neuroimage. 2011 February 14; 54(4): 2779–2788. doi:10.1016/j.neuroimage.2010.10.071.

Improving contrast to noise ratio of resonance frequency contrast images (phase images) using balanced steady-state free precession

Jongho Lee[1], **Masaki Fukunaga**[1,2], and **Jeff H. Duyn**[1]

[1] Advanced MRI Section, Laboratory for Functional and Molecular Imaging, National Institute of Neurological Disorders and Stroke, National Institutes of Health, Bethesda, Maryland [2] Biofunctional Imaging, WPI Immunology Frontier Research Center, Osaka University, Osaka, Japan

Abstract

Recent MRI studies have exploited subtle magnetic susceptibility differences between brain tissues to improve anatomical contrast and resolution. These susceptibility differences lead to resonance frequency shifts which can be visualized by reconstructing the signal phase in conventional gradient echo (GRE) acquisition techniques. In this work, a method is proposed to improve the contrast to noise ratio per unit time (CNR efficiency) of anatomical MRI based on resonance frequency contrast. The method, based on the balanced steady state free precession (bSSFP) MRI acquisition technique, was evaluated in its ability to generate contrast between gray and white matter in human brain at 3T and 7T. The results show substantially improved CNR efficiency of bSSFP phase images (2.85 ± 0.21 times at 3 T and 1.71 ± 0.11 times at 7 T) compared to the GRE data in a limited spatial area. This limited spatial coverage is attributed to the sensitivity of bSSFP to macroscopic B_0 inhomogeneities. With this CNR improvement, high resolution bSSFP phase images (resolution = $0.3 \times 0.3 \times 2$ mm^3, acquisition time = 10 min) acquired at 3 T had sufficient CNR to allow the visualization of cortical laminar structures in *in-vivo* human primary visual cortex. Practical application of the proposed method may require improvement of B_0 homogeneity and stability by additional preparatory scans and/or compensation schemes such as respiration and drift compensation. Without these additions, the CNR benefits of the method may be limited to studies at low field or limited regions of interest.

Keywords

ultra high field MRI; MR microscopy; balanced SSFP and GRE sequence comparison; 7 Tesla

Introduction

Ultra high field MRI (≥7 T) is exquisitely sensitive to subtle variations in magnetic susceptibility, a fact that has been exploited to improve resolution and contrast in BOLD

Address correspondence to: Jongho Lee, 9000 Rockville Pike, Building 10, Room B1D723A, Bethesda, MD 20892-1065, TEL: (301) 451-9919, FAX: (301) 408-1981, jonghoyi@mail.nih.gov.

fMRI (Yacoub et al., 2001; Ugurbil et al., 2003; Hu and Norris, 2004) and susceptibility-weighted anatomical imaging (Deistung et al., 2008; Rauscher et al., 2008; Yao et al., 2009). Particularly large gains have been observed for anatomical imaging based on resonance frequency contrast, derived from the phase of gradient echo (GRE) images (Duyn et al., 2007; Abduljalil et al., 2003; Rauscher et al., 2005; Hammond et al., 2008; Koopmans et al., 2008). GRE image phase allows sufficient contrast to noise ratio (CNR) and spatial resolution to reveal the laminar architecture of the cortex (Duyn et al., 2007; Marques et al., 2009) and the major fiber bundles of white matter (Hernandez et al., 2009; Lee et al., 2010b). Much of the observed resonance frequency variation across the brain can be directly attributed to variations in the concentrations of iron (Fukunaga et al., 2010; Duyn et al., 2007; Haacke et al., 2005), myelin (Fukunaga et al., 2010; Ogg et al., 1999), and deoxyhemoglobin (Lee et al., 2010a; Petridou et al., 2010; Marques et al., 2009; Sedlacik et al., 2008; Haacke et al., 2004). Other contrast mechanisms such as chemical exchange (Zhong et al., 2008; Luo et al., 2010; Shmueli et al., 2010) and microstructural orientation (He and Yablonskiy, 2009; Lee et al., 2010b) have also been suggested and investigated.

The technique of choice for the measurement of resonance frequency shifts across brain regions is a conventional gradient echo sequence with substantial T_2^*-weighting, allowing resonance frequency shifts to translate into substantial phase accumulation. As a result, the reconstructed phase image is sensitive to local variations in resonance frequency. GRE provides robust and efficient data acquisition when the echo time and readout duration are matched to the prevalent tissue T_2^* values, and flip angles to the prevalent Ernst angles.

Despite the efficiency of GRE, the technique sacrifices a certain amount of sensitivity (and potentially CNR) due to the spoiling of transverse magnetization after each data acquisition period. Omitting this spoiling, as is done in balanced Steady State Free Precession (bSSFP) sequences (Carr, 1958; Oppelt et al., 1986; Zur et al., 1988), may improve signal to noise ratio (SNR) and has been demonstrated to be advantageous for certain applications (Scheffler and Lehnhardt, 2003). The bSSFP sequence allows signal contribution from multiple echo pathways and results in higher SNR efficiency compared to GRE (Hargreaves et al., 2003; Kornaat et al., 2005; Krug et al., 2007; Nayak et al., 2005). Additionally, it provides a unique $\sqrt{T_2/T_1}$ contrast that can be particularly beneficial in certain applications (Hargreaves et al., 2003; Nayak et al., 2005). However, with a few exceptions such as flow imaging (Overall et al., 2002; Markl et al., 2003; Grinstead and Sinha, 2005), neuronal current measurement (Buracas et al., 2008) and bSSFP fMRI (Miller et al., 2003; Scheffler et al., 2001) where strong phase contrast has been demonstrated (Lee et al., 2007), most of the bSSFP studies have utilized only the image magnitude and ignored the image phase.

In this study, we propose the application of bSSFP for the measurement of anatomy-based resonance frequency variations across the human brain. We demonstrate that this new approach provides significantly higher CNR efficiency (i.e. CNR per unit time) for a limited spatial coverage compared to conventional GRE sequences. The limited spatial coverage owes to the sensitivity of bSSFP to B_0 inhomogeneity that may originate from such sources as macroscopic susceptibility variation and imperfect shimming. Using this method, cortical structures in *in-vivo* human visual cortex can be visualized even at fields as low as 3 Tesla.

Material and Methods

bSSFP phase amplification

In bSSFP, both magnitude and phase of the signal are dependent on the local resonance frequency. An example of this dependency is illustrated in Fig. 1 for the parameters of TR = 10 ms, TE = 5 ms, flip angle (FA) = 23° (Fig. 1a and 1b) and 3° (Fig. 1c and 1d), T_1 = 1500 ms, T_2 = 70 ms, and off-resonance frequency = −50 Hz to 50 Hz. One of the unique features of these magnetization profiles is observed near the on-resonance frequency where a large phase transition over a narrow frequency band occurs (the shaded area in Fig. 1d). The slope of this phase transition is very steep (132° of phase difference from −5 Hz to 5 Hz, and 96° from −2.5 Hz to 2.5 Hz when T_2 = 70 ms; 110° of phase difference from −5 Hz to 5 Hz, and 71° from −2.5 Hz to 2.5 Hz when T_2 = 45 ms) and is a function of only T_2 (see Fig. 2 for the effects of T_1, T_2, flip angle, and TE on the bSSFP profile). Therefore, if a small frequency difference between different tissue types (*e.g.*, gray and white matter) exists over this phase transition frequency band, it will create a substantial contrast in the phase image. For instance, a 1.5 Hz frequency difference, which is approximately the average frequency difference between gray and white matter at 3 T, results in a phase difference of up to 36° (for T_2 = 70 ms) independent of TE (even at a commonly used TE of 5 ms or less). For comparison, a GRE acquisition would require a TE of 67 ms to achieve the same phase contrast. Hence, bSSFP can provide significant phase amplification for acquisitions with a short TE. Combined with this strong phase contrast, the inherently high SNR of bSSFP (Hargreaves et al., 2003;Kornaat et al., 2005;Krug et al., 2007;Nayak et al., 2005) makes it uniquely suitable for the detection of frequency differences between tissue types.

Computer simulation

To further investigate the properties of phase contrast in bSSFP, additional computer simulations were performed. The default parameters for these simulations were TR = 10 ms, TE = 5 ms, flip angle = 3°, off-resonance frequency = −50 Hz to 50 Hz, and frequency shift between gray and white matter = 1.4 Hz at 3 T and 4 Hz at 7 T. The T_1 values for 3 T were 1523 ms in gray matter and 843 ms in white matter and for 7 T, 2132 ms in gray matter and 1220 ms in white matter (Rooney et al., 2007). The T_2 values for 3 T were 110 ms in gray matter and 80 ms in white matter (Wansapura et al., 1999) and 60 ms in both gray and white matter at 7 T (Michaeli et al., 2002). In the 7 T simulation, the signal was increased by a factor of 7/3 compared to 3 T to account for the increased proton polarization. The bSSFP profiles were generated by steady-state approximation of the Bloch equations (Patz, 1988). To estimate phase contrast, the gray and white matter bSSFP profiles were simulated based on the T_1, T_2 and the scan parameters. The T_2^* effects were expected to be minimal and therefore ignored (Scheffler and Hennig, 2003) After that the profiles were shifted by a given frequency offset and the white matter phase profile was subtracted from the gray matter phase profile. This resulted in a phase contrast over a range of frequency offsets. To calculate CNR, the phase contrast profile was multiplied point by point by the mean value of the shifted gray and white matter magnitude profiles, assuming noise to be 1.

Several properties of the bSSFP phase contrast were investigated. First, the phase contrast and phase CNR were simulated over a range of off-resonance frequencies for various amounts of resonance frequency contrast. The resonance frequency shifts used for the simulation were 1, 2, 4, 5 and 10 Hz for 7 T and 0.4, 0.9, 1.4, 2.1, and 4.3 Hz for 3 T. These particular ranges were chosen to cover the typical GM-WM frequency contrast observed at each field (4 Hz and 1.4 Hz at 7 T and 3 T respectively), with the 3 T values approximately 3/7 scaled down from the 7 T values. After that, the CNR dependency on a flip angle was investigated. The flip angle was varied over 0° to 90° in every 0.1°. The mean CNR of the Full-Width-Half-Maximum (FWHM) phase contrast frequency band was plotted as function of a flip angle. This result was compared to that of GRE. For the GRE simulation, the phase contrast was defined as $2\pi\cdot\Delta f\cdot TE$ where Δf is a resonance frequency shift. The signal magnitude was calculated from $\exp(-TE/T_2^*)\cdot[(1-\exp(-TR/T_1))\sin(\alpha)]/[1-\exp(-TR/T_1)\cos(\alpha)]$, where α is a flip angle. The TE was set to approximately the prevalent T_2^* in brain tissue, using 45 ms at 3 T (Wansapura et al., 1999) and 30 ms at 7 T (Li et al., 2006). The TR was set to 66.8 ms at 3 T and 50 ms at 7 T, which were the same values used in the MRI experiments (see below). The signal magnitude values were calculated using gray and white matter relaxation parameters respectively and then they were averaged for a mean signal magnitude. The CNR of GRE was derived by multiplying the phase contrast by the mean signal magnitude. The dependence of phase contrast on T_2 was also evaluated. Three T_2 values (90, 110, and 130 ms at 3 T and 40, 60 and 80 ms at 7 T) of gray matter were simulated while fixing the white matter T_2 (80 ms at 3 T and 60 ms at 7 T).

Subjects and Scanners

The CNR efficiency of bSSFP and GRE was compared in human brain at 3 T and 7 T. A total ten subjects (five for 3 T and five for 7 T) were scanned under IRB-approved protocols after providing written consent. Additional scans were acquired on two subjects to demonstrate high resolution imaging at 3 T. Scans were performed on General Electric 3 T and 7 T EXCITE MRI systems with 40 mT/m gradient strength, 150 mT/m/ms gradient slew rate, and equipped with 16 and 32 channel Nova Medical head coils respectively.

Scan parameters for bSSFP and GRE comparison

For a proper comparison between bSSFP and GRE experiments, scan parameters were optimized for each sequence separately. Parameters included in this optimization were (1) TR, (2) TE, (3) flip angle, (4) data acquisition bandwidth and acquisition window duration, and (5) readout duty cycle. To reduce any RF excitation profile discrepancy that might occur when 2D and 3D acquisitions were compared, both 3 T scans were performed as 3D acquisitions whereas the 7 T data sets were both acquired in single slice 2D mode.

To optimize CNR efficiency in the GRE acquisitions, the echo times and the duration of the readout acquisition window were approximately matched to the average T_2^* value of brain tissue (values see above). The GRE TR (66.8 ms at 3 T and 50 ms at 7 T) was chosen to be rather short to minimize scan time and consequently reduce the effects of drift and instabilities. As these values were well below T_1, they did not compromise the attainable CNR efficiency. RF flip angles were set to the Ernst angles based on T_1 = 1300 ms at 3 T and T_1 = 1700 ms at 7 T. A gradient spoiling scheme was used with a constant gradient spoiler at the slice selection axis and no RF spoiling was used.

For bSSFP scans, the TR was set to 10 ms to allow a relatively long acquisition window duration and the acquisition window duration and acquisition bandwidth were chosen to fully utilize available time within the TR to maximize SNR. The echo time (4.5 ms at 3 T and 4.8 ms at 7 T) was not important in the transition band of bSSFP because the phase transition and signal magnitude do not change significantly over the readout (Fig. 2g and 2h). The flip angle was set to 3° to optimize the signal near the on-resonance frequency (Fig. 3e and 3g). A commonly used RF phase cycling ($\pi - 0 - \pi - 0 - \ldots$) in bSSFP was not applied to keep the phase transition band at the on-resonance frequency.

The scan time was 6.68 times longer with GRE (400.8 sec) compared to bSSFP (60 sec) at 3 T and 5 times longer with GRE (72 sec) at 7 T compared to bSSFP (14.4 sec). Other parameters such as FOV, resolution, and slice thickness were the same in both GRE and bSSFP sequences. For all scans, data acquisitions started after 6 seconds of pulsing (i.e., "dummy" scans) to allow the spin system to reach a steady state. The parameters for all scans are summarized in Table 1.

For additional comparison between GRE and bSSFP, one subject was scanned with the same scan time (2 min.) at 3 T. All other scan parameters were kept the same as Table 1 except the number of slices (6 slices for GRE and 40 slices for bSSFP), which were adjusted to match the scan times.

Additional considerations for 7 T

Due to the RF wavelength effects (Vaughan et al., 2001) substantial spatial variations in B_1, and therefore flip angle, are expected at 7 T. To avoid suboptimal SNR due to this flip angle variability and inaccurate flip angle calibration, multiple flip angle data were collected at 7 T both for the GRE and bSSFP sequences. This procedure may not be necessary when accurate B_1 information is available, e.g. through simulations or B_1 field mapping methods. Initially, the applied flip angles were stepped by 8° for GRE and 4° for bSSFP; once peak signal in a manually drawn region of interest (ROI) in primary sensory-motor area was reached, the steps were refined to 2° for GRE and 1° for bSSFP.

Another issue potentially affecting image quality particularly for the bSSFP technique is B_0 drift. At 3 T, this drift was relatively small and reproducible and therefore allowed compensation based on a drift estimate (measured once in a phantom) by adjusting RF transmit frequency during the acquisition (Miller et al., 2006). At 7 T, however, the drift was significantly larger and more variable presumably due to larger amount of passive shim material used in the scanner. Hence the compensation applied at 3T was not performed at 7 T. To avoid the suboptimal results from this problem, five different center frequencies (−6 Hz, −3 Hz, 0 Hz, +3 Hz, and +6 Hz) were acquired at 7 T in bSSFP. After shifting the center frequencies, 3 sec worth of idle time was used (Miller, 2010). For subsequent image analysis and comparison with GRE, only one center frequency dataset that was closest to the NMR resonance frequency was analyzed.

The multiple center frequency strategy used for bSSFP reduces overall CNR efficiency; it may not be necessary if the drift is compensated by real-time drift compensation methods (Lee et al., 2006; Wu et al., 2007). Another source for B_0 fluctuation is respiration (Noll and Schneider, 1994) and its detrimental effect on bSSFP scans has been investigated in bSSFP fMRI (Lee et al., 2006). In this study, real time shimming was used at 7 T to reduce the respiration induced image degradation (van Gelderen et al., 2007). However this method did not compensate for B_0 drift from non-respiratory sources.

Data acquisition

For 3 T GRE and bSSFP comparison scans, the primary visual cortex area was localized using a 3 plane localizer and localized B_0 shimming (up to first order) was performed focusing on the visual cortex (FOV = 24 × 24 × 2.4 cm^3, resolution = 3 × 3 × 2 mm^3, TR = 30 ms, TE_1 = 3 ms, TE_2 = 7 ms, flip angle = 13°, and total scan time = 28 sec). This shimming was repeated 2 – 3 times to ensure convergence. A short bSSFP scout scan (FOV = 20 × 15 × 2.4 cm^3, resolution = 1 × 1 × 4 mm^3, TR = 10 ms, flip angle = 3°) was acquired using a range of resonance frequencies (−6 Hz, −3 Hz, 0 Hz, +3 Hz, and +6 Hz; 1 sec idle time after each frequency shift; total scan time = 55 sec) to ensure the ROI was close to on-resonance. After that, bSSFP and GRE scans were acquired to compare resonance frequency contrast.

For high resolution bSSFP images at 3 T, the scan parameters were FOV = 15 × 15 cm^2, resolution = 0.3 × 0.3 × 2 mm^3, TR = 9.4 ms, TE = 4.3 ms, BW = ±50 kHz, flip angle = 3°, number of slice = 20, number of repetition = 6, and scan time = 10 min with additional 6 sec of dummy scan. The same shimming procedure and scout scan were performed as mentioned before.

For 7 T GRE and bSSFP comparison scans, the primary sensory-motor cortex area was localized using a 3-plane localizer and global shimming was performed on the whole brain. A real-time shimming was used to reduce the respiration-induced resonance frequency shift (van Gelderen et al., 2007). Note that the sensory-motor area was targeted to avoid significant respiration effects. However, the problem was largely mitigated by the real-time shimming. After real-time shimming, the flip angle was calibrated based on the coil that has the highest signal in the targeted primary sensory-motor areas. Linear shims were optimized over the primary sensory-motor cortex area in one hemisphere of the brain (parameters: FOV = 20 × 20 × 2 cm^3, 2.5 × 2.5 × 2 mm^3, TR = 30 ms, TE_1 = 3 ms, TE_2 = 7 ms, flip angle = 11°, and total scan time = 24 sec). A short bSSFP scout scan (FOV = 24 × 18 cm^2 or 20 × 15 cm^2, resolution = 2 × 2 mm^2 or 1 × 1 mm^2, slice thickness = 2 mm, 4 averages, TR = 10 ms, flip angle = 3°, different center frequency acquired = −10 Hz, −5 Hz, 0 Hz, +5 Hz, and +10 Hz and total scan time = 25 or 37 sec with a 3 sec initial dummy scan and 1 sec transition between different center frequencies) was performed to verify the shimming. The bSSFP and GRE scans were performed repeatedly with varying flip angle to avoid suboptimal SNR due to uncertainty in the actual flip angle, which may have resulted from B_1 inhomogeneity and inaccurate flip angle calibration. Before each repetition in bSSFP, the center frequency of the scanner was shifted by +6 Hz to compensate for the scanner drift. If the drift was not stable and the contrast was suboptimal, the scan was repeated with an adjusted center frequency. However, all the experimental images, plots and SNR and CNR results presented below are from single center frequency data.

Data processing

The individual coil data were reconstructed by Fourier transformation after which the resulting complex images of individual coils were scaled by coil sensitivity and corrected for coil phase offsets. The phase offset of the individual coils, which was measured as the mean phase value of the central voxels, was predetermined in a GRE phantom scan. The coil sensitivity was determined based on the noise variance measured at the background area outside the brain. The magnitude images were generated by root-sum-of-squares coil combining. The phase images were derived from the complex sum of the sensitivity-weighted and phase offset corrected individual coil data (de Zwart et al., 2002). Phase unwrapping was done within a brain area of interest (*e.g.*, occipital lobe at 3 T and motor and sensory areas at 7 T). The unwrapped phase images were filtered using a 2D Gaussian filter (FWHM = 21 voxels) to remove the large scale phase variation.

All the images were spatially aligned before further analysis. Gray and white matter ROIs were drawn manually for the quantification of the resonance frequency contrast, SNR, and CNR. An ROI was first drawn based on bSSFP phase images in high contrast gray and white matter areas. Then the ROI was refined on GRE phase images generating a separate ROI for GRE to avoid any remaining misalignment errors due to subject motions between the scans. Hence both bSSFP ROI and GRE ROI covered almost the same areas with tissue matching optimized for each dataset. The gray and white matter CNR of the phase images was calculated as follows: the contrast was determined by the mean value of the gray matter ROI subtracted by the mean of the white matter ROI. After that the CNR was calculated by multiplying this contrast with the SNR of the magnitude image as suggested previously (Duyn et al., 2007). The SNR of magnitude image was estimated by the average signal intensity in the gray and white matter ROIs divided by the SD of the background noise corrected by $\sqrt{2-\pi/2}$ (Gudbjartsson and Patz, 1995).

Results

The simulation results are shown in Fig. 3. Close to the NMR resonance frequency, the bSSFP method shows substantial phase contrasts (Fig. 3a – 3d). Both phase contrast and phase CNR increase with increasing resonance frequency shifts. The bandwidth of the phase contrast and phase CNR also widen for larger frequency shifts. For a 1.4 Hz frequency shift, which is approximately the gray and white matter frequency difference at 3 T, the FWHM bandwidth of the phase contrast is 3.9 Hz. This increases to 7.8 Hz for a equivalent 4 Hz frequency difference at 7 T. The dependence of the phase CNR over a range of flip angles is plotted in Fig. 3e – 3h for both GRE and bSSFP. The optimum flip angles are 2.2° at 3 T and 2.5° at 7 T in bSSFP. For GRE, the values are 19.9° and 14.5° for 3 T and 7 T respectively. In the actual experiment, bSSFP flip angles were rounded up to 3° to conform to the accepted values of the scanner. As indicated from Fig. 3e – 3h, the phase CNR of bSSFP shows a relatively strong dependence on a flip angle. Since the optimum flip angle is much smaller in bSSFP than GRE, however, the relative B_1 variation will be also smaller in bSSFP. Assuming a 50 % flip angle variation of the maximum flip angle (the shaded areas in Fig. 3e – 3h), the minimum CNR of this range in bSSFP is 81% of the maximum at 3 T (82% at 7 T) whereas it is 80% at 3 T (79% at 7 T) in GRE. Hence once flip angle is properly calibrated, the relative sensitivity to B_1 inhomogeneity is similar in GRE and bSSFP. When the mean phase contrast is assumed to be the average value of the phase contrast in the FWHM bandwidth in bSSFP and the optimum flip angle is used for both bSSFP and GRE, the CNR gain of the bSSFP over GRE reaches values of 3.5 at 3 T and 2.8 at 7 T based on the simulation. Figure 3i and 3j show the phase contrast dependence on T_2 value. When the gray matter T_2 value moves away from the white matter T_2 (80 ms at 3 T and 60 ms at 7 T), the asymmetry of the phase contrast becomes larger.

Sample bSSFP and GRE images at 3 T are shown in Figure 4. The bSSFP magnitude image (Fig. 4a) shows high signal intensity at the posterior side of the brain where the shim was targeted. In this area, strong resonance frequency contrast (0.443 ± 0.062 rad averaged over all subjects) between the gray and white matter is observed (Fig. 4b and 4c) as expected from the steepness of the bSSFP phase profile (Fig. 1c and 1d). A relatively large area reveals a high level of resonance frequency contrast despite only using zeroth and first order shims. The strong reduction of the contrast observed outside this area is attributed to the sensitivity of the bSSFP phase contrast to off-resonance frequencies as shown in Fig. 3a and 3b. The large frequency contrast observed in the bSSFP image at TE = 4.5 ms demonstrates the phase amplification effect at the transition band of bSSFP; the gray and white matter contrast is even larger than that of the GRE image (0.386 ± 0.045 rad when averaged over all subjects, Fig. 4f and 4g) acquired at TE = 45 ms. The CNR of bSSFP phase image was slightly higher (19.8 ± 3.7 when averaged over all subjects) than that of GRE (18.1 ± 3.8 when averaged in all subjects). When scaled to CNR per unit time (i.e. CNR efficiency) by taking into account the scan time difference (1 min for bSSFP and 6.68 min for GRE), the bSSFP phase images yielded 2.85 ± 0.21 higher CNR efficiency compared to GRE images. This is slightly below the 3.5-fold improvement predicted by the simulations. The results of individual subjects are summaried in Table 2.

One major difference between the two methods is the frequency contrast in regions with CSF; the bSSFP phase image shows large negative phase in CSF whereas the GRE image shows close to zero contrast. This is attributed to the fact that CSF has a long T_2 which makes the bSSFP phase transtion extremely steep (Fig. 2d), thereby magnifying frequency contrast. This effect helps to distinguish the gray matter and CSF boundary better in the bSSFP images.

The average gray and white matter CNR of the bSSFP magnitude images was −1.5 ± 1.6 and that of the GRE magnitude images was 0.8 ± 1.9 indicating minimal magnitude contrast between gray and white matter in both scans. This is also evident in Fig. 4a and 4e.

At 7 T, the per unit time CNR advantage of the bSSFP method was reduced but still significant (overall 1.71 ± 0.11, Table 3). The gain is smaller than the 2.8-fold improvement predicted by the simulations. This discrepancy may originate from a number of factors, including differences between simulated and actual tissue parameters and deterioration of bSSFP performance due to residual B_0 variability related to drift and respiration. The bSSFP

NIH-PA Author Manuscript

NIH-PA Author Manuscript

phase images (Fig. 5b and 5c) show similar contrast (TE = 4.8 ms for bSSFP and TE = 30 ms for GRE) with slightly lower SNR and CNR. The lower SNR and CNR are due to five times shorter scan time for bSSFP as compared to that of GRE. In bSSFP, phase contrast was observed in a limited area due to B_0 and B_1 inhomogeneity. To avoid the effect of these issues on the bSSFP CNR values, the ROIs for gray and white matters were confined to a small region.

The average gray and white matter CNR of the bSSFP magnitude images was −1.3 ± 1.0 whereas that of the GRE magnitude images was −0.8 ± 1.3 demonstrating magnitude contrast was lower than phase contrast. This agrees the 3 T findings and previously published results (Duyn et al., 2007). The negative sign in the magnitude contrast indicates the opposite contrast between the magnitude and phase contrasts (i.e. the phase image shows positive contrast in gray matter whereas the magnitude image shows lower signal intensity in gray matter as shown in Fig. 5. Note that the color scale in phase images is reversed and positive phase is darker than negative phase).

Figure 6 shows the gray and white matter CNRs over multiple flip angles in all subjects. The ROIs for these plots are the same regional ROIs used for the CNR comparison in Fig. 5. The results indicate that CNR is relativley uniform across the flip angles in both GRE and bSSFP. This apparent discrepancy from the simulation results (Fig. 3g and 3h) can, at least partly, be explained by the B_1 inhomogenity within the ROIs; as the flip angle changes some areas may move closer to the optimum flip angle whereas the other areas may move away from the optimum flip angle. The x-axis shown in Fig. 6 represents nominal flip angles used in the scans. The actual mean flip angles in the ROI may be somewhat different from the nominal values due to inaccurate flip angle calibration and B_1 inhomogeneity. Note that some of the CNR curves do not show a peak within the range of applied flip angles. This is because the decision for the optimum flip angle during the experiments was based on a rough ROI that may not have exactly matched to the ROIs used for analysis. Also, the mean signal intensity was used instead of CNR in the opimimum flip angle estimation.

Results of the 3 T high resolution experiment are shown in Figure 7. In certain cortical areas, a laminar structure resembling the line of Gennari is visible (red arrow), consistent with earlier work at 7 T (Duyn et al., 2007).

In Supplementary Figure 1, both GRE and bSSFP images at 3 T acquired within the same scan time (2 min.) are shown. The bSSFP phase contrast image clearly demonstrates improved CNR compared to GRE.

Discussion and Conclusions

In this work, we proposed and evaluated the use of the bSSFP acquisition technique to improve anatomical contrast in resonance frequency-based MRI of the human brain. Compared to GRE techniques, the method led to CNR efficiency improvements of 2.85 ± 0.21 and 1.71 ± 0.11 at 3 T and 7 T respectively. A significant limitation of the method is reduced spatial coverage due to B_0 inhomogeneity. This could be improved by several techniques discussed below. Robust performance of the bSSFP method may also require additional preparatory scans and/or respiration and drift compensation methods, particularly at 7 T. Despite these caveats, this new approach may enable the visualization of even finer structures than possible with conventional methods. Alternatively it may allow the exquisite details earlier obtained at 7 T with conventional methods to become visible at 3 T.

Spatial off-resonance

One drawback of the proposed method is the limited spatial coverage due to its restricted dynamic range. The phase amplification effect only occurs over a small frequency range, outside of which the contrast is strongly reduced. Off-resonance due to macroscopic susceptibility variations and/or imperfect shimming may severely limit the extent of the region with optimal contrast. In Figure 4, for example, when the area of the gray and white matter ROIs was enlarged to cover the whole phase image area shown in Fig. 4b and 4f (the new gray and white matter ROIs are shown in Supplementary Figure 2), the average phase contrast in bSSFP was reduced from 0.454 rad (the original ROIs shown in Fig. 4d) to 0.261 rad (the new ROIs shown Supplementary Figure 2). This resulted in a deceased CNR efficiency gain from 2.63 to 1.65. This off-resonance problem becomes more challenging at high field where frequency spreads increase proportionally. A number of methods may be applied to improve the spatial coverage. First, improved higher order shims and local shims (Kim et al., 2002;Wilson et al., 2002;Hsu and Glover, 2005) can be used. The current study was performed using only up to the first order shims. Hence the spatial coverage will be improved if higher order shims and local shims are included. Second, a better shim algorithm can be applied. For example, The minimization of the maximum off-resonance shimming method (Lee et al., 2009) incorporated with region growing algorithm may have potential for increasing the spatial coverage. Combined with these, a parallel excitation can be used to compensate for the spatial B_0 and B_1 inhomogeneity (Heilman et al., 2009). It is also possible to use multiple shifted center frequency scans (Miller et al., 2006;Bangerter et al., 2004) to improve the spatial coverage at the expense of CNR efficiency. For example, when five center frequencies each of which is shifted by 4 Hz are acquired at 3 T, the FWHM bandwidth for the combined phase contrast is increased to 20.3 Hz and the theoretical CNR efficiency gain becomes 2.15. At 7 T, when three different center frequencies are acquired with each center frequency shifted by 8 Hz, the FWHM bandwidth is 22.1 Hz and the gain reduces to 1.95. An example of a multiple center frequency combined image from the 7 T experiment is shown in Supplementary Figure 3. The image shows improved spatial coverage compared to the single center frequency image in Fig. 5b

Temporal (respiration and drift) off-resonance

Respiration induced B_0 field variation (Noll and Schneider, 1994) and B_0 field drift due to passive shim material, cryostat and gradient coil heating (Foerster et al., 2005) can also induce contrast degradation in bSSFP and effectively shifts the region of optimal contrast over time. These effects have been studied in fMRI and a real-time compensation method has been suggested (Lee et al., 2006; Wu et al., 2007). In the current study, an analogous real-time method that compensates for respiration has been used at 7 T (van Gelderen et al., 2007). However, the method did not take into account (non-respiratory) drift effect. A real time compensation method that compensates for both respiration-induced field variations and instrument drift (Lee et al., 2006) was not implemented for this work because of a scheduled scanner system change at our site. The drift was small and predictable at 3 T and was precompensated (Miller et al., 2006). At 7 T, however, the drift was much larger and more difficult to accurately predict presumably due to large number of passive shim sets used in the scanner. For this reason, in order to minimize the effects of this drift, the total scan time at 7 T was limited to a few seconds. The severe drift problem at 7 T may have led to partially reduced CNR gain obtained with the new method compared to that observed at 3T. Consequently, proper correction of both respiration and drift may lead to further CNR improvements.

Future work

In this study, multiple short preparation scans such as localized shimming (28 s at 3 T and 24 s at 7 T), real time shimming (2 min. only at 7 T) and scout scans (55 s at 3 T and 25 – 37 s at 7 T) were performed to obtain optimal SSFP performance. At 7 T, multiple data acquisitions using several flip angles and center frequencies were also used. These scans were performed to verify the maximum CNR efficiency improvement achievable by the new bSSFP method. For future applications, some of these scans may not be necessary. At 3 T, the scout scan proved unnecessary since the drift was not significant; the localized shimming result was valid for the main scan. Hence the bSSFP method can be acquired right after a localized shimming without any other preparatory scans. At 7 T, if a real time drift compensation method is used, one may not need the scout scan and multiple center frequency acquisition. The multiple flip angle acquisition at 7 T can be replaced by a B_1 field map method. Therefore the combination of the drift compensation and B_1 mapping will significantly reduce the total scan time at 7 T.

The localized shimming performed here was important to acquire phase contrast using the proposed bSSFP method, and it can be improved in several ways. First, the scan time can be shortened using a spiral (Kim et al., 2002) or segmented EPI acquisition. Also, one can program the shim method to show the extent of phase contrast area and/or to inform the necessary number of multiple center frequency acquisitions to cover a certain ROI.

Supplementary Material

Refer to Web version on PubMed Central for supplementary material.

Acknowledgments

This research was supported (in part) by the Intramural Research Program of the NIH, NINDS.

References

Abduljalil AM, Schmalbrock P, Novak V, Chakeres DW. Enhanced gray and white matter contrast of phase susceptibility-weighted images in ultra-high-field magnetic resonance imaging. J Magn Reson Imaging. 2003; 18(3):284–290. [PubMed: 12938122]

Bangerter NK, Hargreaves BA, Vasanawala SS, Pauly JM, Gold GE, Nishimura DG. Analysis of multiple-acquisition SSFP. Magn Reson Med. 2004; 51(5):1038–1047. [PubMed: 15122688]

Buracas GT, Liu TT, Buxton RB, Frank LR, Wong EC. Imaging periodic currents using alternating balanced steady-state free precession. Magn Reson Med. 2008; 59(1):140–148. [PubMed: 18050317]

Carr HY. Steady-state free precession in nuclear magnetic resonance. Physical Review. 1958; 112(5): 1693–1701.

de Zwart JA, van Gelderen P, Kellman P, Duyn JH. Application of sensitivity-encoded echo-planar imaging for blood oxygen level-dependent functional brain imaging. Magn Reson Med. 2002; 48(6):1011–1020. [PubMed: 12465111]

Deistung A, Rauscher A, Sedlacik J, Stadler J, Witoszynskyj S, Reichenbach JR. Susceptibility weighted imaging at ultra high magnetic field strengths: Theoretical considerations and experimental results. Magn Reson Med. 2008; 60(5):1155–1168. [PubMed: 18956467]

Duyn JH, van Gelderen P, Li TQ, de Zwart JA, Koretsky AP, Fukunaga M. High-field MRI of brain cortical substructure based on signal phase. Proc Natl Acad Sci USA. 2007; 104(28):11796–11801. [PubMed: 17586684]

Foerster BU, Tomasi D, Caparelli EC. Magnetic field shift due to mechanical vibration in functional magnetic resonance imaging. Magn Reson Med. 2005; 54(5):1261–1267. [PubMed: 16215962]

Fukunaga M, Li TQ, van Gelderen P, de Zwart JA, Shmueli K, Yao B, Lee J, Maric D, Aronova MA, Zhang G. Layer-specific variation of iron content in cerebral cortex as a source of MRI contrast. Proc Natl Acad Sci U S A. 2010; 107(8):3834–3839. [PubMed: 20133720]

Grinstead J, Sinha S. In-plane velocity encoding with coherent steady-state imaging. Magn Reson Med. 2005; 54(1):138–145. [PubMed: 15968674]

Gudbjartsson H, Patz S. The Rician distribution of noisy MRI data. Magn Reson Med. 1995; 34(6): 910–914. [PubMed: 8598820]

Haacke EM, Cheng NYC, House MJ, Liu Q, Neelavalli J, Ogg RJ, Khan A, Ayaz M, Kirsch W, Obenaus A. Imaging iron stores in the brain using magnetic resonance imaging. Magn Reson Imaging. 2005; 23(1):1–25. [PubMed: 15733784]

Haacke EM, Xu Y, Cheng YC, Reichenbach JR. Susceptibility weighted imaging (SWI). Magn Reson Med. 2004; 52(3):612–618. [PubMed: 15334582]

Hammond KE, Lupo JM, Xu D, Metcalf M, Kelley DAC, Pelletier D, Chang SM, Mukherjee P, Vigneron DB, Nelson SJ. Development of a robust method for generating 7.0 T multichannel phase images of the brain with application to normal volunteers and patients with neurological diseases. Neuroimage. 2008; 39(4):1682–1692. [PubMed: 18096412]

Hargreaves BA, Gold GE, Beaulieu CF, Vasanawala SS, Nishimura DG, Pauly JM. Comparison of new sequences for high-resolution cartilage imaging. Magn Reson Med. 2003; 49(4):700–709. [PubMed: 12652541]

He X, Yablonskiy DA. Biophysical mechanisms of phase contrast in gradient echo MRI. Proc Natl Acad Sci USA. 2009; 106(32):13558–13563. [PubMed: 19628691]

Heilman, JA.; Derakhshan, JJ.; Riffe, MJ.; Gudino, N.; Tkach, J.; Flask, CA.; Duerk, JL.; Griswold, MA. B0 and B1 Correction Using the Inherent Degrees of Freedom of a Multi-Channel Transmit Array. Proceedings of the 17th Annual Meeting of ISMRM; Hololulu, HI. 2009. p. 251

Hernandez, E.; Mackay, A.; Rauscher, A. The relationship between susceptibility weighted phase and white matter fiber orientation. Proceedings of the 17th Annual Meeting of ISMRM; Honolulu, Hawaii. 2009. p. 953

Hsu JJ, Glover GH. Mitigation of susceptibility-induced signal loss in neuroimaging using localized shim coils. Magn Reson Med. 2005; 53(2):243–248. [PubMed: 15678531]

Hu X, Norris DG. Advances in high-field magnetic resonance imaging. Annu Rev Biomed Eng. 2004; 6:157–184. [PubMed: 15255766]

Kim DH, Adalsteinsson E, Glover GH, Spielman DM. Regularized higher-order in vivo shimming. Magn Reson Med. 2002; 48(4):715–722. [PubMed: 12353290]

Koopmans PJ, Manniesing R, Niessen WJ, Viergever MA, Barth M. MR venography of the human brain using susceptibility weighted imaging at very high field strength. MAGMA. 2008; 21:149–158. [PubMed: 18188626]

Kornaat PR, Reeder SB, Koo S, Brittain JH, Yu H, Andriacchi TP, Gold GE. MR imaging of articular cartilage at 1.5 T and 3.0 T: Comparison of SPGR and SSFP sequences. Osteoarthr Cartilage. 2005; 13(4):338–344.

Krug R, Carballido-Gamio J, Banerjee S, Stahl R, Carvajal L, Xu D, Vigneron D, Kelley DAC, Link TM, Majumdar S. In vivo bone and cartilage MRI using fully-balanced steady-state free-precession at 7 tesla. Magn Reson Med. 2007; 58(6):1294–1298. [PubMed: 17957777]

Lee J, Hirano Y, Fukunaga M, Silva AC, Duyn JH. On the contribution of deoxy-hemoglobin to MRI gray-white matter phase contrast at high field. Neuroimage. 2010a; 49(1):193–198. [PubMed: 19619663]

Lee J, Lustig M, Kim D, Pauly JM. Improved shim method based on the minimization of the maximum off-resonance frequency for balanced steady-state free precession (bSSFP). Magn Reson Med. 2009; 61(6):1500–1506. [PubMed: 19319895]

Lee J, Santos JM, Conolly SM, Miller KL, Hargreaves BA, Pauly JM. Respiration-induced B0 field fluctuation compensation in balanced SSFP: Real-time approach for transition-band SSFP fMRI. Magn Reson Med. 2006; 55(5):1197–1201. [PubMed: 16598728]

Lee J, Shahram M, Schwartzman A, Pauly JM. Complex data analysis in high-resolution SSFP fMRI. Magn Reson Med. 2007; 57(5):905–917. [PubMed: 17457883]

Lee J, Shmueli K, Fukunaga M, van Gelderen P, Merkle H, Silva AC, Duyn JH. Sensitivity of MRI resonance frequency to the orientation of brain tissue microstructure. Proc Natl Acad Sci U S A. 2010b; 107(11):5130–5135. [PubMed: 20202922]

Li TQ, van Gelderen P, Merkle H, Talagala L, Koretsky AP, Duyn J. Extensive heterogeneity in white matter intensity in high-resolution T2*-weighted MRI of the human brain at 7.0 T. Neuroimage. 2006; 32(3):1032–1040. [PubMed: 16854600]

Luo J, He X, d'Avignon DA, Ackerman JJH, Yablonskiy DA. Protein-induced water 1H MR frequency shifts: Contributions from magnetic susceptibility and exchange effects. J Magn Reson. 2010; 202(1):102–108. [PubMed: 19879785]

Markl M, Alley MT, Elkins CJ, Pelc NJ. Flow effects in balanced steady state free precession imaging. Magn Reson Med. 2003; 50(5):892–903. [PubMed: 14586999]

Marques JP, Maddage R, Mlynarik V, Gruetter R. On the origin of the MR image phase contrast: An in vivo MR microscopy study of the rat brain at 14.1 T. Neuroimage. 2009; 46:345–352. [PubMed: 19254768]

Michaeli S, Garwood M, Zhu XH, DelaBarre L, Andersen P, Adriany G, Merkle H, Ugurbil K, Chen W. Proton T2 relaxation study of water, N-acetylaspartate, and creatine in human brain using Hahn and Carr-Purcell spin echoes at 4T and 7T. Magn Reson Med. 2002; 47(4):629–633. [PubMed: 11948722]

Miller KL. Asymmetries of the balanced SSFP profile. Part I: Theory and observation. Magn Reson Med. 2010; 63(2):385–395. [PubMed: 20099328]

Miller KL, Hargreaves BA, Lee J, Ress D, de Charms CR, Pauly JM. Functional brain imaging using a blood oxygenation sensitive steady state. Magn Reson Med. 2003; 50(4):675–683. [PubMed: 14523951]

Miller KL, Smith SM, Jezzard P, Pauly JM. High-Resolution FMRI at 1.5 T Using Balanced SSFP. Magn Reson Med. 2006; 55:161–170. [PubMed: 16345040]

Nayak KS, Hargreaves BA, Hu BS, Nishimura DG, Pauly JM, Meyer CH. Spiral balanced steady-state free precession cardiac imaging. Magn Reson Med. 2005; 53:1468–1473. [PubMed: 15906302]

Noll, DC.; Schneider, W. Respiration artifacts in functional brain imaging: sources of signal variation and compensation strategies. Proceedings of the Society of Magnetic Resonance; San Francisco, USA. 1994. p. 647

Ogg RJ, Langston JW, Haacke EM, Steen RG, Taylor JS. The correlation between phase shifts in gradient-echo MR images and regional brain iron concentration. Magn Reson Imaging. 1999; 17(8):1141–1148. [PubMed: 10499676]

Oppelt A, Graumann R, Barfuss H, Fischer H, Hartl W, Shajor W. FISP- new fast MRI pulse sequence. Electromedica. 1986; 54:15–18.

Overall WR, Conolly SM, Nishimura DG, Hu BS. Oscillating dual-equilibrium steady-state angiography. Magn Reson Med. 2002; 47(3):513–522. [PubMed: 11870838]

Patz S. Some factors that influence the steady state in steady-state free precession. Magn Reson Imaging. 1988; 6(4):405–413. [PubMed: 3185134]

Petridou N, Wharton SJ, Lotfipour A, Gowland P, Bowtell R. Investigating the effect of blood susceptibility on phase contrast in the human brain. Neuroimage. 2010; 50(2):491–498. [PubMed: 20026280]

Rauscher A, Barth M, Herrmann KH, Witoszynskyj S, Deistung A, Reichenbach JR. Improved elimination of phase effects from background field inhomogeneities for susceptibility weighted imaging at high magnetic field strengths. Magn Reson Imaging. 2008; 26(8):1145–1151. [PubMed: 18524525]

Rauscher A, Sedlacik J, Barth M, Mentzel HJ, Reichenbach JR. Magnetic susceptibility-weighted MR phase imaging of the human brain. AJNR. 2005; 26(4):736. [PubMed: 15814914]

Rooney WD, Johnson G, Li X, Cohen ER, Kim SG, Ugurbil K, Springer CS Jr. Magnetic field and tissue dependencies of human brain longitudinal 1H2O relaxation in vivo. Magn Reson Med. 2007; 57(2):308–318. [PubMed: 17260370]

Scheffler K, Hennig J. Is TrueFISP a gradient-echo or a spin-echo sequence? Magn Reson Med. 2003; 49(2):395–397. [PubMed: 12541263]

Scheffler K, Lehnhardt S. Principles and applications of balanced SSFP techniques. European Radiology. 2003; 13(11):2409–2418. [PubMed: 12928954]

Scheffler K, Seifritz E, Bilecen D, Venkatesan R, Hennig J, Deimling M, Haacke EM. Detection of BOLD changes by means of a frequency-sensitive trueFISP technique: preliminary results. NMR Biomed. 2001; 14(7–8):490–496. [PubMed: 11746942]

Sedlacik J, Kutschbach C, Rauscher A, Deistung A, Reichenbach JR. Investigation of the influence of carbon dioxide concentrations on cerebral physiology by susceptibility-weighted magnetic resonance imaging (SWI). Neuroimage. 2008; 43(1):36–43. [PubMed: 18678260]

Shmueli K, Dodd SJ, Li TQ, Duyn JH. The contribution of chemical exchange to MRI frequency shifts in brain tissue. Magn Reson Med. 2010 available online.

Ugurbil K, Adriany G, Andersen P, Chen W, Garwood M, Gruetter R, Henry PG, Kim SG, Lieu H, Tkac I. Ultrahigh field magnetic resonance imaging and spectroscopy. Magn Reson Imaging. 2003; 21(10):1263–1281. [PubMed: 14725934]

van Gelderen P, de Zwart JA, Starewicz P, Hinks RS, Duyn JH. Real-time shimming to compensate for respiration-induced B0 fluctuations. Magn Reson Med. 2007; 57(2):362–368. [PubMed: 17260378]

Vaughan JT, Garwood M, Collins CM, Liu W, DelaBarre L, Adriany G, Andersen P, Merkle H, Goebel R, Smith MB. 7 T vs. 4 T: RF power, homogeneity, and signal-to-noise comparison in head images. Magn Reson Med. 2001; 46(1):24–30. [PubMed: 11443707]

Wansapura JP, Holland SK, Dunn RS, Ball WS Jr. NMR relaxation times in the human brain at 3.0 Tesla. J Magn Reson Imaging. 1999; 9(4):531–538. [PubMed: 10232510]

Wilson JL, Jenkinson M, Jezzard P. Optimization of static field homogeneity in human brain using diamagnetic passive shims. Magn Reson Med. 2002; 48(5):906–914. [PubMed: 12418007]

Wu ML, Wu PH, Huang TY, Shih YY, Chou MC, Liu HS, Chung HW, Chen CY. Frequency stabilization using infinite impulse response filtering for SSFP fMRI at 3T. Magn Reson Med. 2007; 57(2):369–379. [PubMed: 17260379]

Yacoub E, Shmuel A, Pfeuffer J, Van De Moortele PF, Adriany G, Andersen P, Vaughan JT, Merkle H, Ugurbil K, Hu X. Imaging brain function in humans at 7 Tesla. Magn Reson Med. 2001; 45(4): 588–594. [PubMed: 11283986]

Yao B, Li TQ, Gelderen PV, Shmueli K, de Zwart JA, Duyn JH. Susceptibility contrast in high field MRI of human brain as a function of tissue iron content. Neuroimage. 2009; 44(4):1259–1266. [PubMed: 19027861]

Zhong K, Leupold J, von Elverfeldt D, Speck O. The molecular basis for gray and white matter contrast in phase imaging. Neuroimage. 2008; 40(4):1561–1566. [PubMed: 18353683]

Zur Y, Stokar S, Bendel P. An analysis of fast imaging sequences with steady-state transverse magnetization refocusing. Magn Reson Med. 1988; 6(2):175–193. [PubMed: 3367775]

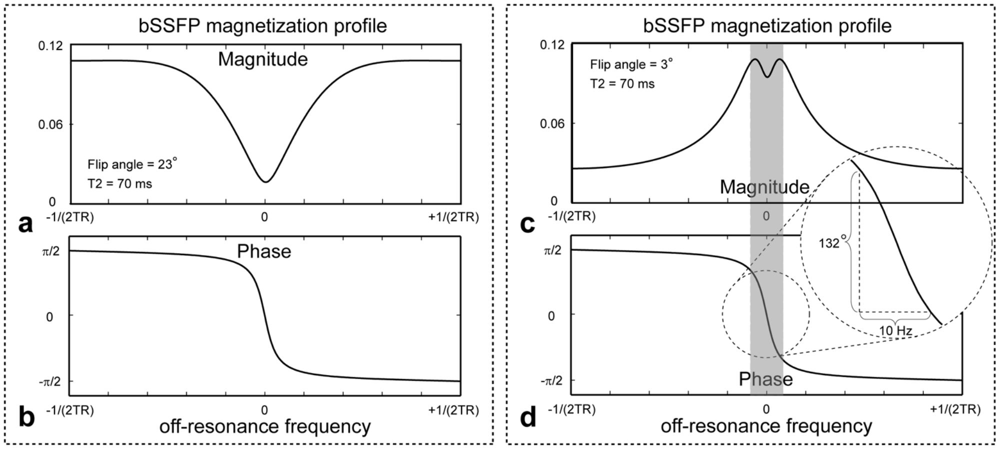

Figure 1.

Balanced SSFP magnetization profiles. Magnitude (a and c) and phase (b and d) signals are plotted as a function of resonance frequency of spins. When the flip angle is in medium range (23°), a magnitude dip exists around on-resonance (a). This shape is inverted for the very small flip angle case (3°) as shown in (c). A commonly used RF phase cycling (π – 0 – π – 0 – …) has not been applied for either flip angle. Near the resonance frequency there is a sharp phase transition (gray area) that may create a large phase contrast for a small frequency difference.

NIH-PA Author Manuscript
NIH-PA Author Manuscript

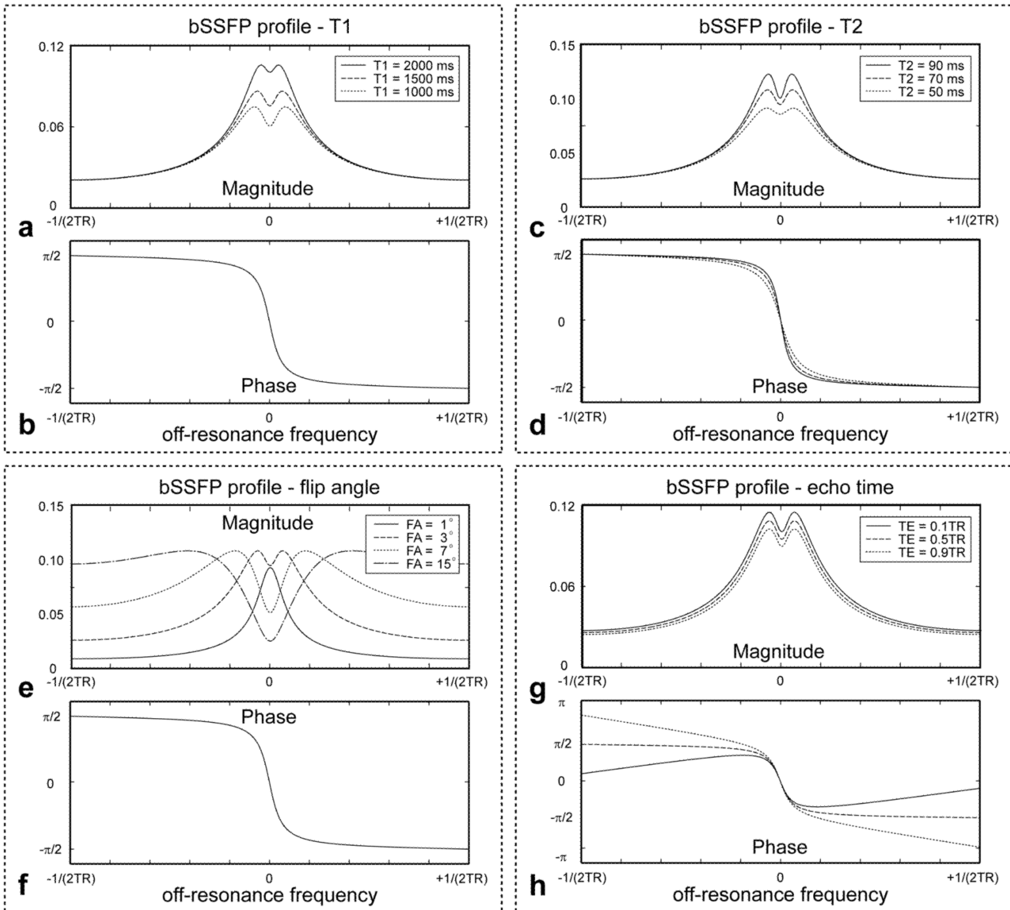

Figure 2.

Balanced SSFP magnetization profiles for multiple T_1 (a and b), T_2 (c and d), flip angle (e and f) and TE (g and h) values. The default values for the simulation were TR = 10 ms, TE = 5 ms, flip angle = 3°, T_1 = 1500 ms, T_2 = 70 ms, and off-resonance frequency = −50 Hz to 50 Hz. Despite large changes in the shape of the magnitude profile, the phase transition near the resonance frequency is only affected by T_2 values. A long T_2 induces sharper phase transition whereas a short T_2 reduces the phase slope. This phase transition variation generates additional frequency contrast when T_2 values are significantly different. For example, clear delineation of gray matter and CSF boundary is observed in bSSFP phase images compared to GRE phase images (Fig. 4, 5 and 7).

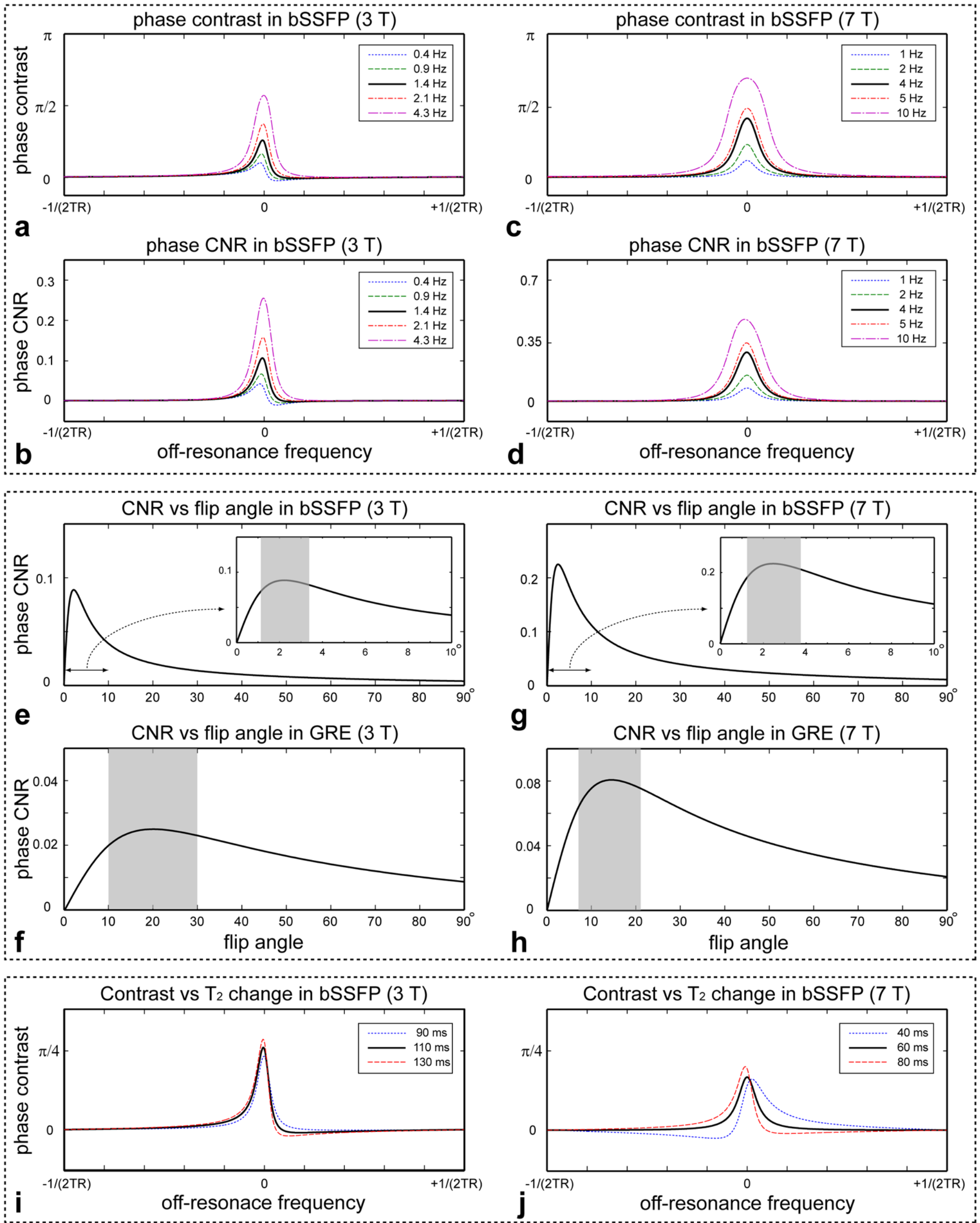

Figure 3.

Simulations results. (a–d) Balanced SSFP phase contrast at 3 T (a) and 7 T (c) and phase CNR at 3 T (b) and at 7 T (d) over a 1/TR frequency range for various resonance frequency shifts. The solid black line represents the results of the gray and white matter frequency contrasts (1.4 Hz at 3 T and 4 Hz at 7 T). (e–h) Phase CNR dependence on a RF flip angle in bSSFP at 3 T (e), bSSFP at 7 T (g), GRE at 3 T (f), and GRE at 7 T (h). The inset plots show a zoomed range between 0° and 10°. The shaded areas represent 50% flip angle variation ranges from the optimum flip angles. (i and j) Phase contrast for multiple gray matter T_2 values. For white matter, the default T_2 value (80 ms at 3 T and 60 ms at 7 T) was used.

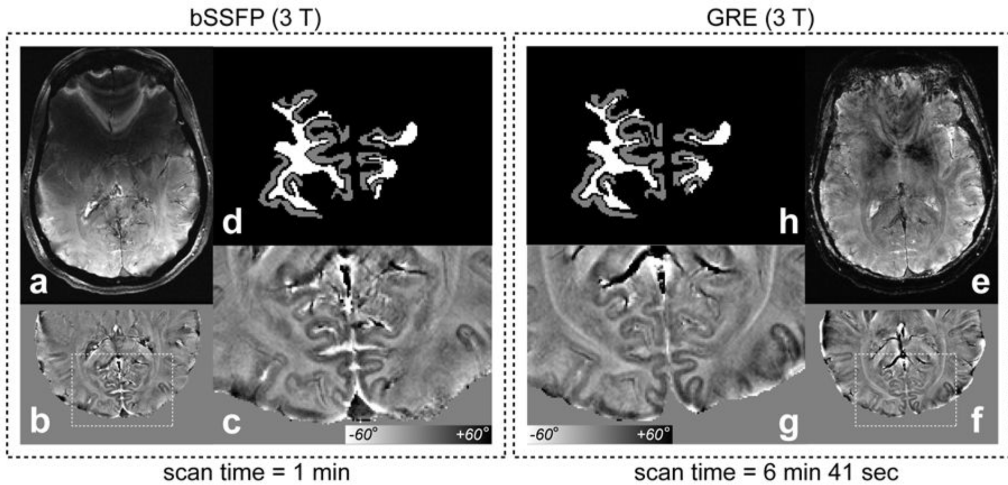

Figure 4.

Comparison of bSSFP and GRE images at 3 Tesla. (a) bSSFP magnitude image. High signal is observed in an area that is close to resonance. (b) bSSFP phase image. High contrast is seen close to resonance in a similar area where magnitude signal is high (compare with a). As can be seen from comparison with the GRE phase image in (f) contrast is lost away from resonance. (c) Expansion of the dotted area in (b). (d) bSSFP ROIs (white for white matter and gray for gray matter) for quantification. (e–h) GRE equivalents of (a–d). The CNR of the phase image is slightly higher in the bSSFP image compared to GRE. When corrected for difference in scan time (1 min for bSSFP and 6.68 min for GRE), the CNR efficiency of bSSFP is 2.85 ± 0.21 higher than that of GRE (averaged over all five subjects).

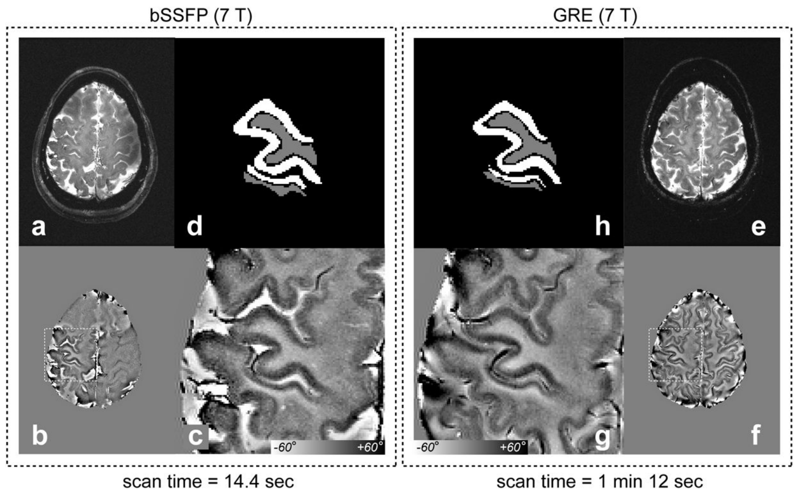

Figure 5.

Comparison of bSSFP and GRE images at 7 Tesla. (a) bSSFP magnitude image. (b) bSSFP phase image. The contrast exists in limited areas due to B_0 and B_1 inhomogeneities. (c) bSSFP phase image zoomed in the dotted rectangle area in (b). (d) bSSFP ROIs (white for white matter and gray for gray matter) for quantification. (e–h) GRE equivalents of (a–d). The CNR of the phase image is lower in the bSSFP image compared to GRE. However, when corrected for difference in scan time (14.4 sec for bSSFP and 1 min 12 sec for GRE), the CNR efficiency of bSSFP is 1.71 ± 0.11 (when averaged in all subjects) higher than that of GRE.

NIH-PA Author Manuscript
NIH-PA Author Manuscript

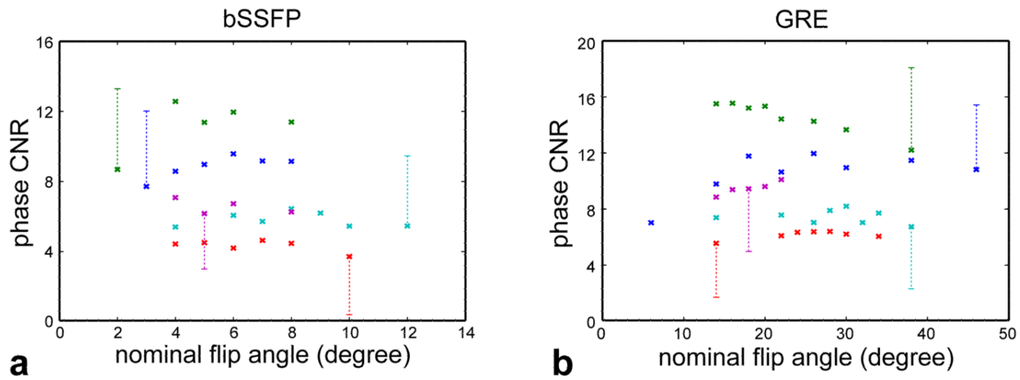

Figure 6.
Phase CNR at 7 T as a function of flip angle in all subjects. Each color represents one subject. The CNR is relatively uniform across a range of flip angles. The x-axis represents nominal flip angle which may be somewhat different from the actual mean flip angle in the ROI.

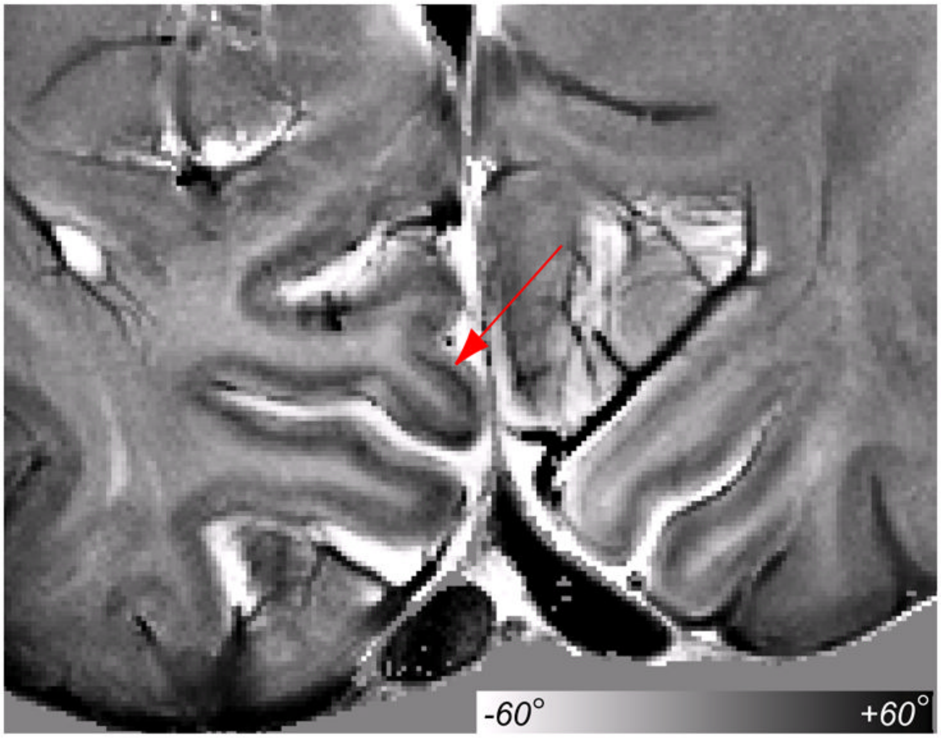

Figure 7.

High resolution bSSFP phase image at 3 T. The bSSFP method provides higher CNR that enables imaging of intracortical structure. The line of Gennari (red arrow) is visible at 3 T in vivo in a relatively short scan time (10 min).

NIH-PA Author Manuscript
NIH-PA Author Manuscript

Table 1

Scan parameters for the comparison of GRE and bSSFP at 3 T and 7 T

	TR	TE	Flip angle[a]	Band- width	FOV	Resolution	# avg.	Duty cycle[b]	Scan time[c]
GRE 3 T	66.8 ms	45 ms	18°	4.72 kHz	$20 \times 15 \times 4$ cm^3	$0.5 \times 0.5 \times 2$ mm^2	1	63.4 %	400.8 sec
bSSFP 3 T	10 ms	4.5 ms	3°	31.25 kHz	$20 \times 15 \times 4$ cm^3	$0.5 \times 0.5 \times 2$ mm^2	1	64 %	60 sec
GRE 7 T	50 ms	30 ms	14°	8.33 kHz	$24 \times 18 \times 0.2$ cm^3	$0.5 \times 0.5 \times 2$ mm^2	4	57.6%	72 sec
bSSFP 7 T	10 ms	4.8 ms	3°	41.67 kHz	$24 \times 18 \times 0.2$ cm^3	$0.5 \times 0.5 \times 2$ mm^2	4	57.6%	14.4 sec

[a] Flip angles were nominal values. In the 7 T experiment, multiple flip angles were acquired to find maximum CNR.

[b] Duty cycle was calculated as the duration of the data acquisition period divided by TR.

[c] Scan time was the total data acquisition time for a single center frequency excluding the dummy scan period.

NIH-PA Author Manuscript
NIH-PA Author Manuscript

Table 2

Comparison of gray and white matter frequency contrast in bSSFP and GRE at 3 T

3 Tesla	bSSFP (1 min)			GRE (6.68 min)			bSSFP gain[a]
	Contrast (rad)	SNR	CNR	Contrast (rad)	SNR	CNR	
1	0.518	48.6	25.2	0.453	52.0	23.8	2.76
2	0.411	44.0	18.1	0.345	49.6	17.1	2.73
3	0.368	43.8	16.1	0.346	44.4	15.4	2.72
4	0.493	44.3	21.9	0.399	50.2	20.1	2.82
5	0.424	41.9	17.8	0.386	37.2	14.3	3.21
Average ± S.D.	0.443 ± 0.062	44.5 ± 2.5	19.8 ± 3.7	0.386 ± 0.045	46.7 ± 6.0	18.1 ± 3.8	2.85 ± 0.21

[a] bSSFP gain is defined as $(\mathrm{CNR}_{\mathrm{bSSFP}} / \sqrt{\mathrm{ScanTime}_{\mathrm{bSSFP}}})/(\mathrm{CNR}_{\mathrm{GRE}} / \sqrt{\mathrm{ScanTime}_{\mathrm{GRE}}})$.

NIH-PA Author Manuscript

NIH-PA Author Manuscript

Table 3

Comparison of gray and white matter frequency contrast in bSSFP and GRE at 7 T

7 Tesla	bSSFP (14.4 sec)			GRE (72 sec)			bSSFP gain[a]
	Contrast (rad)	SNR	CNR	Contrast (rad)	SNR	CNR	
1	0.703	13.6	9.6	0.762	15.7	12.0	1.79
2	0.779	16.1	12.6	0.744	20.9	15.5	1.81
3	0.831	5.6	4.6	0.801	8.0	6.4	1.62
4	0.860	7.5	6.4	0.804	10.2	8.2	1.76
5	0.716	9.9	7.1	0.746	13.5	10.1	1.57
Average	0.778 ± 0.069	10.5 ± 4.3	8.1 ± 3.1	0.771 ± 0.029	13.7 ± 5.0	10.4 ± 3.5	1.71 ± 0.11

[a]bSSFP gain is defined as $(\mathrm{CNR}_{\mathrm{bSSFP}}/\sqrt{\mathrm{ScanTime}_{\mathrm{bSSFP}}})/(\mathrm{CNR}_{\mathrm{GRE}}/\sqrt{\mathrm{ScanTime}_{\mathrm{GRE}}})$.